LIQUEFACTION: STRENGTH AND WAVE-BASED MONITORING

Jong-Sub Lee[1], P.E., Member, ASCE, Gye Chun Cho[2], Member, ASCE,
and J. Carlos Santamarina[3], Member, Geo-Institute,

ABSTRACT: The phenomenon of liquefaction has been extensively studied, yet, the prediction of field performance remains uncertain. The first part of this manuscript presents a detailed analysis of published results to identify robust strength criteria. The second part documents experimental data on the characterization of liquefaction events with P-wave reflection imaging and S-wave transillumination techniques. The relevance of multiple coexisting temporal and spatial scales is highlighted.

INTRODUCTION

Soil response to seismic loading and the associated infrastructure damage have been studied by many prominent researchers for more than 60 years. The underlying microscale mechanisms are relatively well known even though unexpected behavior and emerging phenomena are still being recognized and discovered. Thus, today's state of the art still reflects significant uncertainty; this is particularly the case in deformation prediction not only in the horizontal direction (where the uncertainty is very high), but even in the vertical direction (where there is a clear bound to possible settlements).

The purpose of this manuscript is to analyze post liquefaction shear strength and to explore the potential use of wave-based techniques to monitor liquefaction and post liquefaction response.

[1] Postdoctoral Fellow, Civil and Environmental Engineering, Georgia Institute of Technology, Atlanta, GA 30332, USA.
[2] Assistant Professor, Civil and Environmental Engineering, KAIST, Daejeon 305-701, South Korea.
[3] Professor - Goizueta Chair, Civil and Environmental Engineering, Georgia Institute of Technology, Atlanta, GA 30332, USA. carlos.santamarina@ce.gatech.edu.

POST LIQUEFACTION SHEAR STRENGTH

The dynamic response of a saturated sandy soil to earthquake excitation can be analyzed into two distinct cases. “Flow liquefaction” occurs when the post liquefaction shear strength is lower than the initial deviatoric stress acting at the site, for example in slope stability problems, lateral deformation and flow. On the other hand, the term “cyclic mobility” applies when the initial level of static shear stress is lower than the monotonic shear strength on the critical state line. Typically, cyclic mobility is relevant to level-ground. Table 1 presents a comparative analysis of flow liquefaction and cyclic mobility and the corresponding engineering problems and approaches in each case.

The monotonic critical state response provides a robust framework to understand the development of undrained strength in soils. Figure 1 shows the response of a contractive soil subjected to undrained and drained loading. For simplicity, the path followed by the soil is often captured by its projections on the vertical and horizontal planes, that is the *p’-q* and the *p’-e* projections. To avoid confusion, the interpretation of these projections must recognize the three dimensional nature of the path in the *p’-q-e* space.

Drained and undrained behaviors are intimately related, as can be observed in Figure 2. Figure 2-a shows the deviatoric stress versus strain plot for three sands subjected to drained loading and the corresponding evolution in void ratio. The response under undrained loading is captured in Figure 2-b both in deviatoric stress versus strain, and pore pressure versus strain. The critical state strength is shown in all cases. Note that the variable is the void ratio while the initial effective confinement is kept constant. The transition points in drained behavior observed in the void ratio versus strain plot manifest as transition points as well in the undrained behavior, and they are denoted as the “quasi-steady state condition” or “phase transformation”.

The end points at large strain are the strength values corresponding to the critical state line. Experimental data for blasting sand are presented in Figure 3. The two specimens have similar void ratios. Therefore, the contractive tendency is controlled by the initial effective stress that is applied: the higher the effective stress, the stronger the contractive tendency. As seen in the Figure 3, the specimen subjected to $(\sigma_3')_0$= 320 kPa reaches a peak followed by a structural collapse with the associated generation of pore pressure. After phase transformation, the soil regains its strength once again. Both specimens tend to the same critical state strength, which is determined by the initial void ratio. Clearly, the quasi-steady state strength exhibits high variability both in magnitude and in the strain level at which it manifests. On the other hand, the critical state strength is robust, and it depends on void ratio only, however, it is a large-strain strength.

The comparison between the quasi-steady state line and the critical state line presented in Table 2 is based on published results. It can be concluded from this compilation that the critical state line is virtually not affected by most soil parameters such as initial void ratio, confining stress, initial stress ratio, fabric, prestraining or stress path. However, the quasi-steady state line is affected by all these parameters and many of these parameters can be assessed neither in-situ nor in the laboratory with any degree of certainty.

TABLE 1. Flow liquefaction and cyclic mobility - Comparison.

	Flow Liquefaction	Cyclic Mobility
Behavior	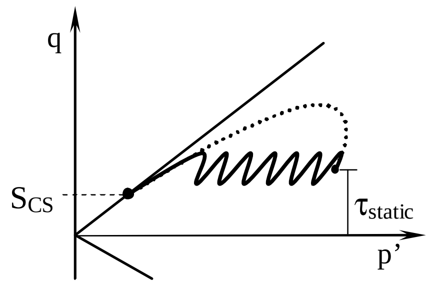	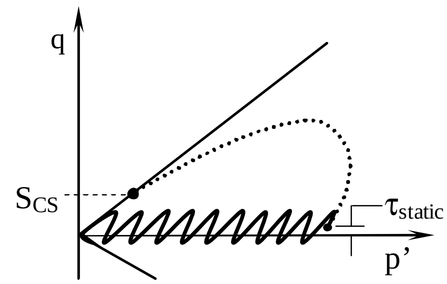
Initial τ	$\tau_{static} \geq S_{CS}$	$\tau_{static} < S_{CS}$
Soil type	Contractive	Low and medium densities
Factors	Not sensitive to initial conditions Depends on σ'_o and e_o Possible effect of loading path May be affected by plastic fines*	Sensitive to - σ'_o and e_o - amplitude excitation - initial stiffness (aging, prestrain, cementation, fabric) - percentage of plastic fines*
Engineering problems	Slope problems Lateral deformation, flow	Level ground Early role in slope instability
Uniqueness	Quite unique Easy determination of steady state line in e-p' space	Many parameters affect strength due to the characteristics of pore water pressure generation
Design approach	Strength is considered	Deformation is considered
Design parameter	Min{$[S_{CS}]_{dr}$, $[S_{CS}]_{und}$}	Strength @ 5% double-amplitude strain @ 15cycles (5% criterion: good for clean and silty sands)

Notes: *The percentage of fines may play a more critical role in field performance than in laboratory measurements (time for *u* dissipation versus earthquake duration).

CS critical state; S_{CS} critical state shear strength on *p'-q* space; *dr* drained condition; *und* undrained condition.

Sources: Alarcon-Guzman et al. 1988; Been 1999; Dobry et al. 1985; Ishihara 1993; Poulos et al. 1985; Seed 1979; Vaid and Thomas 1995; Yoshimine et al. 1999.

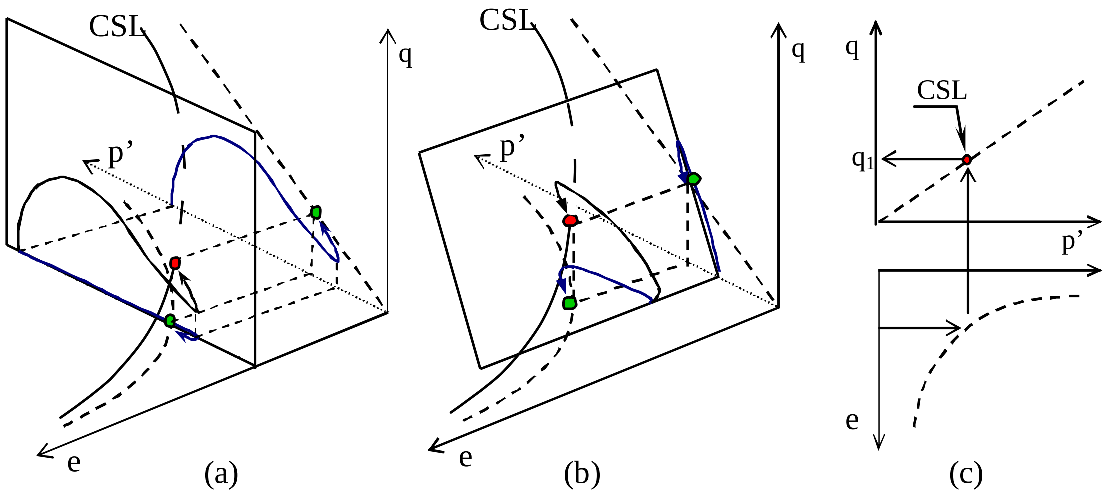

FIG. 1. Monotonic soil behavior in the *p'-q-e* space. (a) Undrained response of a contractive soil. (b) Drained response of a dilative soil. (c) Projections of CSL on *p'-q* and the *p'-e* planes.

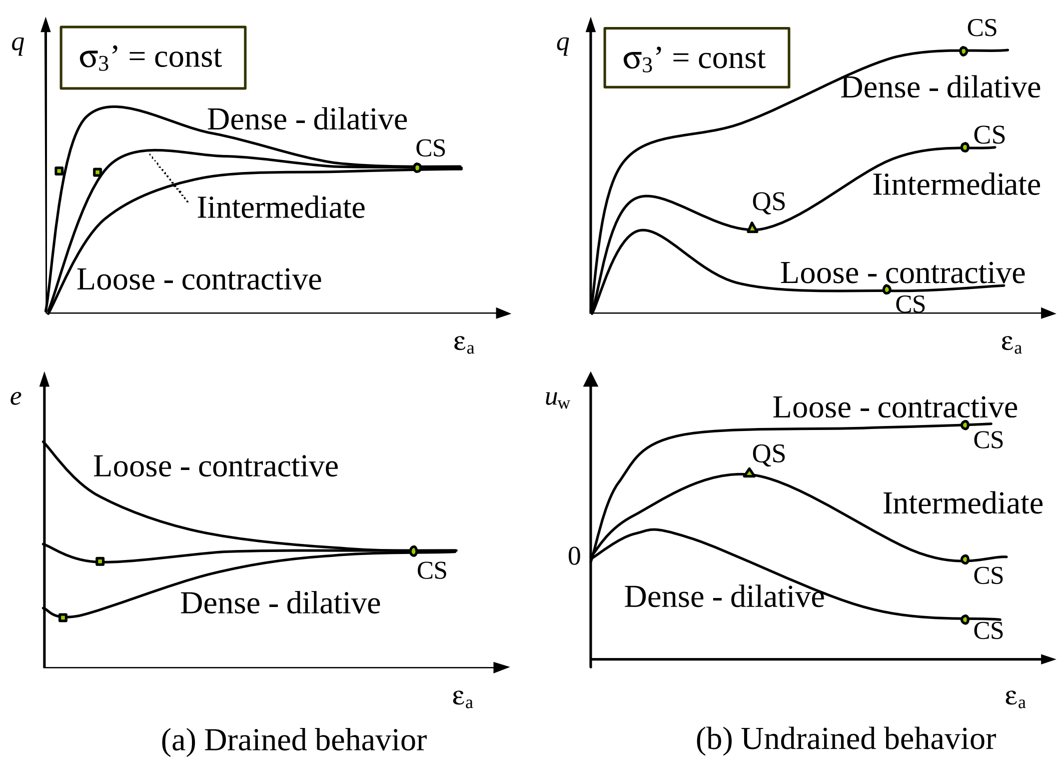

FIG. 2. Quasi-static loading for drained and undrained behavior.

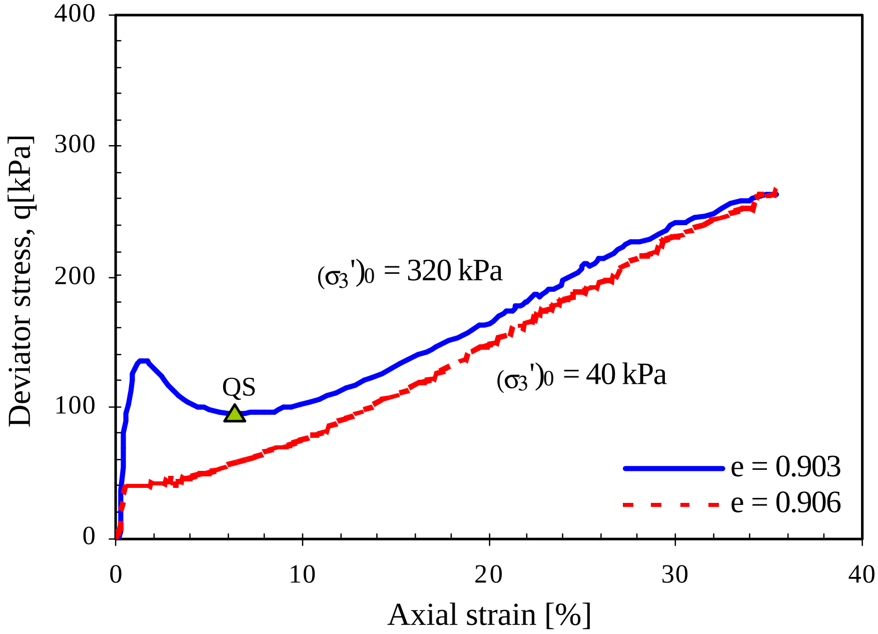

FIG. 3. Undrained triaxial test results for blasting sand at different initial effective confining stresses. Soil properties: e_{max}= 1.025, e_{min}= 0.698, D_{50}= 0.71mm, D_{10}= 0.42mm, Cu= 1.94, Cc= 0.94, Gs= 2.65. Angular sand: R= 0.3 (roundness), S= 0.55 (sphericity). CS friction angle= 32°. Intercept of CSL= 1.099 (at 1 kPa). Slope of CSL= 0.069.

TABLE 2. The critical state and the quasi-steady state lines - Comparison (see Cho 2001 for a detailed analysis).

Parameters	Effect	
	Quasi-steady state line	Critical state line
Initial void ratio (relative density)	Strong effect	No effect (unless localization develops)
Confining stress	Strong effect	No effect
Initial stress ratio (induced anisotropy)	Some effect	No effect
Fabric (inherent anisotropy)	Strong effect	No effect (may trigger localization)
Prestraining (and aging)	Strong effect	No effect
Stress path (mode of loading)	Strong effect	No effect (may trigger localization)
Fines content	Strong effect	Strong effect

Sources: Been et al. 1991; Dobry et al. 1985; Finno et al. 1998; Ishihara 1993; Poulos et al. 1988; Yamamuro and Lade 1995; Yoshimine et al. 1999.

WAVE-BASED CHARACTERIZATION

The propagation of elastic waves provides important information for a wide range of applications ranging from material characterization to medical diagnosis. The P-wave velocity is related to the bulk stiffness of the fluid B_f, the mineral that makes the grains B_g, the mass density of the fluid r_f and the solid mass r_g, and the porosity n,

$$V_P = \sqrt{\frac{M}{\rho}} = \sqrt{\frac{B_f}{\rho_f}} \sqrt{\frac{1}{\left[(1-n)\frac{B_f}{B_g} + n\right]\left[(1-n)\frac{\rho_g}{\rho_f} + n\right]}} \tag{1}$$

On the other hand, the shear wave velocity depends primarily on the shear stiffness of the granular skeleton which is determined by the state of stress in the case of uncemented soils,

$$V_S = \alpha \left(\frac{\sigma'_x + \sigma'_y}{2Pa} \right)^{\beta} \tag{2}$$

where Pa is the atmospheric pressure in the same units as s'. The α-coefficient and the β-exponent are interrelated as β = 0.36-α/700 (Santamarina et al. 2001). General trends for β are: β = 0.16 ~0.20 for rounded smooth particles and dense sands, $\beta \approx 0.25$ for loose sands or anglular sands, β = 0.3 for soft clays, and $\beta \leq 0.15$ for over consolidated clays and cemented soils. When a soil liquefies, the pore pressure increases and the mean effective stress decreases, therefore the shear wave velocity decreases according to Equation 2. In summary, the P-wave velocity provides information about changes in porosity while the S-wave velocity reports changes in effective stress and stiffness (both during liquefaction and during excess pore pressure dissipation).

These concepts are tested with the devices sketched in Figure 4. P-wave imaging is attempted with a submerged specimen made of a homogenous sand bed with an intermediate silt layer of lower permeability (Figure 4-a). The source-receiver piezoelectric pair is scanned over the surface to determine the reflection profile. The set up for shear wave velocity characterization consists of a vertical array of bender elements excited simultaneously by a step signal, and a matching vertical array of bender elements used as receivers across the model (Figure 4-b). Both models are impacted with a hammer to simulate the earthquake excitation.

The P-wave reflection images are shown in Figure 5 before and two days after liquefaction. The depression of the soil-water interface and the upper and lower surface of the silt layer provide insightful information about the effect of liquefaction and post liquefaction densification not only at the surface but in the subsurface. Similar images were obtained several minutes after liquefaction and the formation of a water gap on the lower surface of the silt layer was readily recognized.

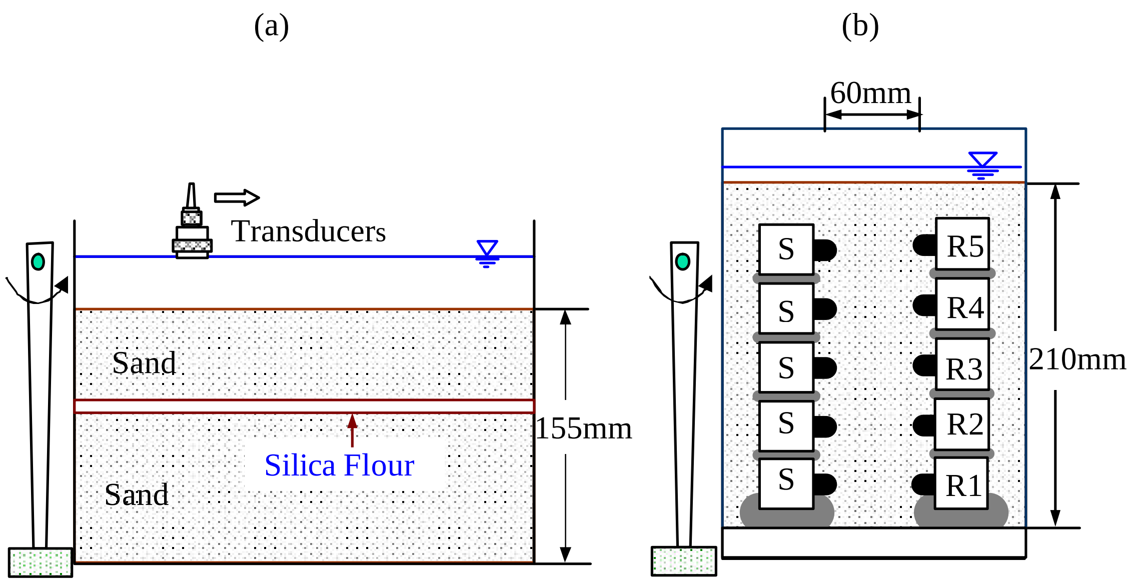

FIG. 4. Devices for P-wave and S-wave liquefaction study. (a) P-wave reflection imaging. (b) S-wave trans-illumination. S and R: bender elements used as sources and receivers (see Lee 2001 for a detailed description of these experimentals and results).

Figure 6 shows the evolution of shear wave signatures on the lower bender element before and after the impact. Clear signals are observed before impact. However, the signal vanishes while the soil remains liquefied, and it gradually recovers as pore pressure dissipation takes place (Note: the vibration itself lasted 10ms). The data gathered with all bender elements is summarized in Figure 7 in terms of velocity. It can be seen that transducers at all depths show the massive development of liquefaction. The longer duration of liquefaction in the shallower layers confirms the upwards pore water migration during re-sedimentation.

Settlement is the macroscale manifestation of resedimentation. The cumulative settlement with successive impact-drainage cycles is shown in Figure 8. Results show that settlement occurs even after forty independent liquefaction-drainage events.

CLOSING REMARKS

The post liquefaction shear strength can be estimated within the framework of critical state soil mechanic, where the monotonic stress path is an upper envelop of the cyclic stress path. The critical state line is (relatively) unique with respect to the initial state of stress, initial fabric, and even minor digenetic effects. This is not the case for the quasi-steady state line. The determination of the critical state line must be conducted with conditions that prevent post peak strain softening behavior and strain localization. Therefore, the best method to obtain the critical state parameters in the laboratory is to use contractive homogeneous specimens subjected to drained shear.

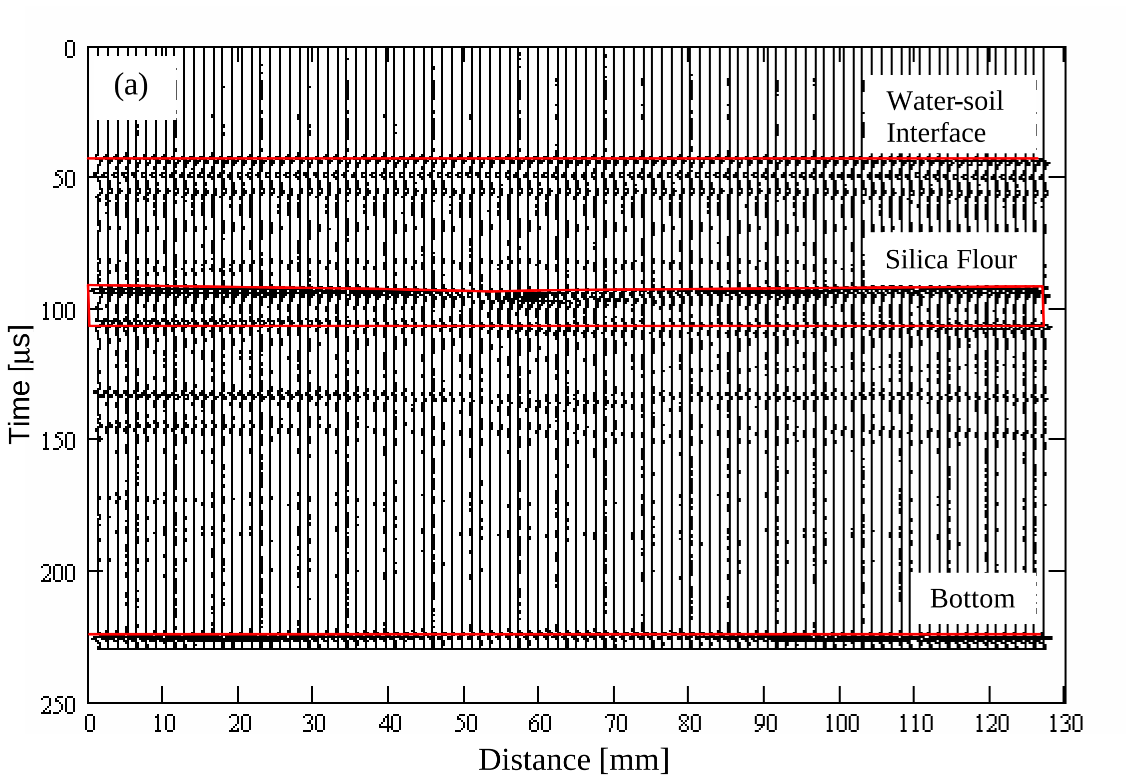

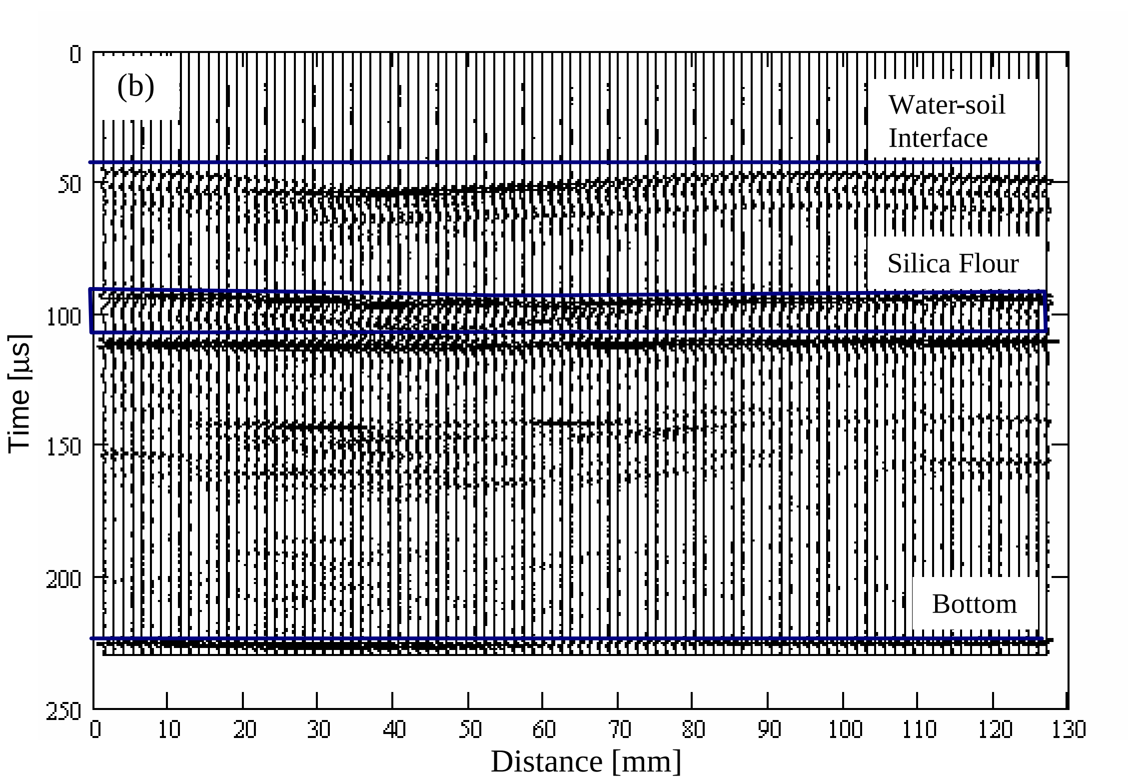

FIG. 5. P-wave reflection images. (a) Before liquefaction. (b) 2 days after liquefaction; lines indicate the position of soil layers before liquefaction.

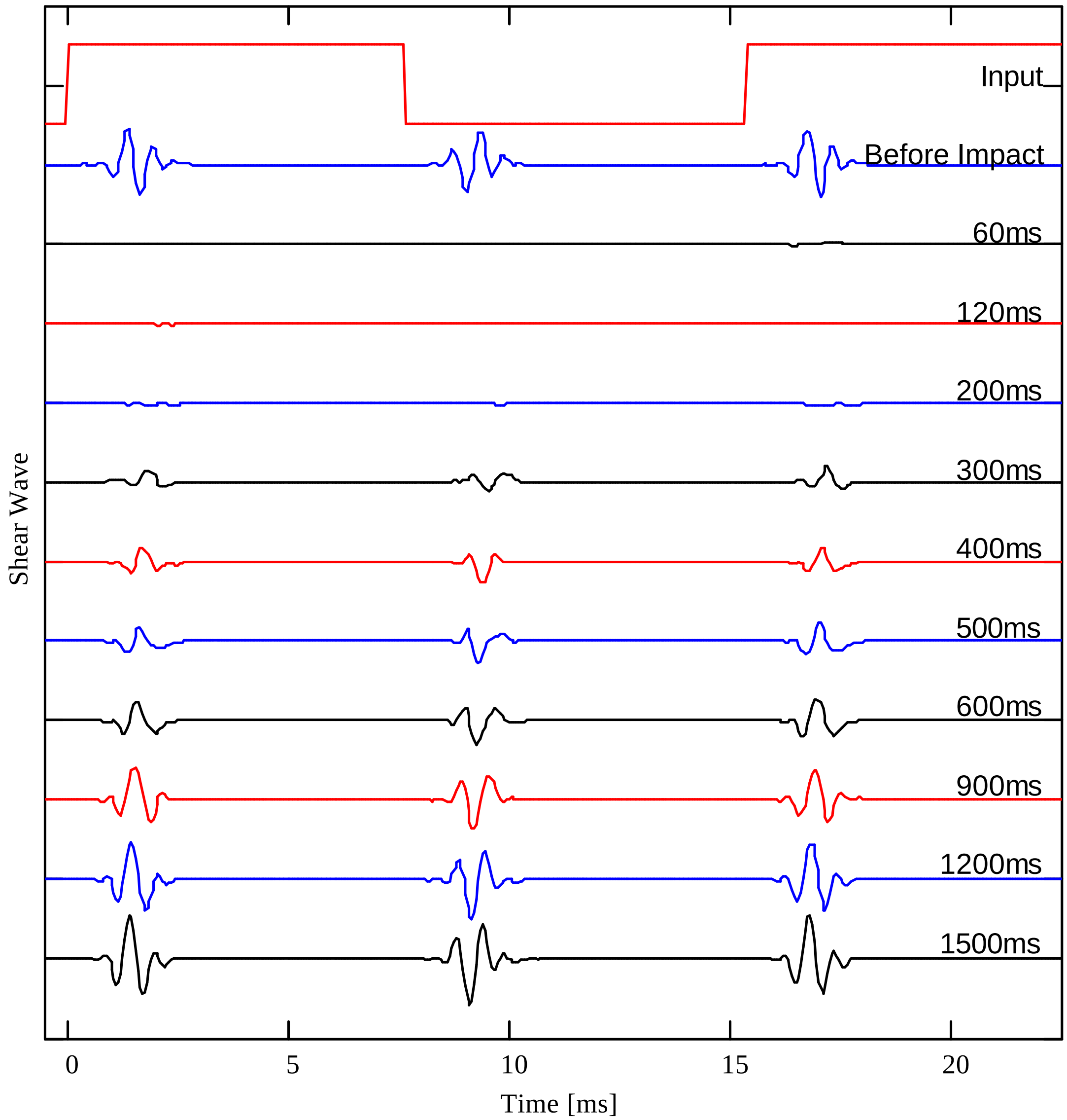

FIG. 6. Snapshots of the S-wave signals registered at the bender element (R1) at different times.

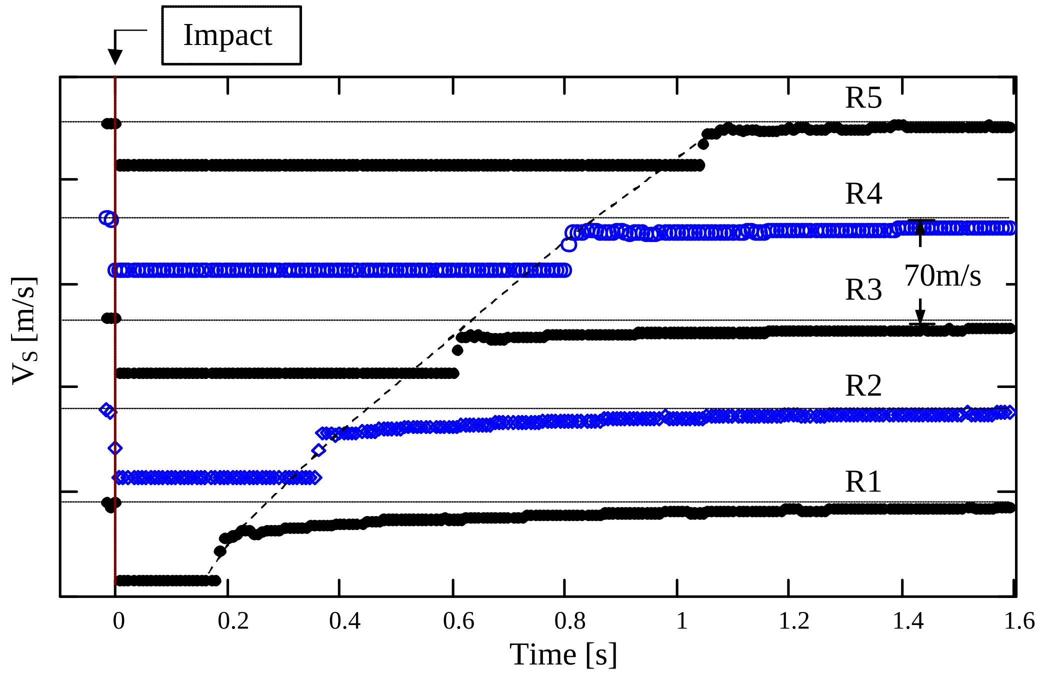

FIG. 7. Evolution of shear wave velocity with time during liquefaction and excess pore water dissipation.

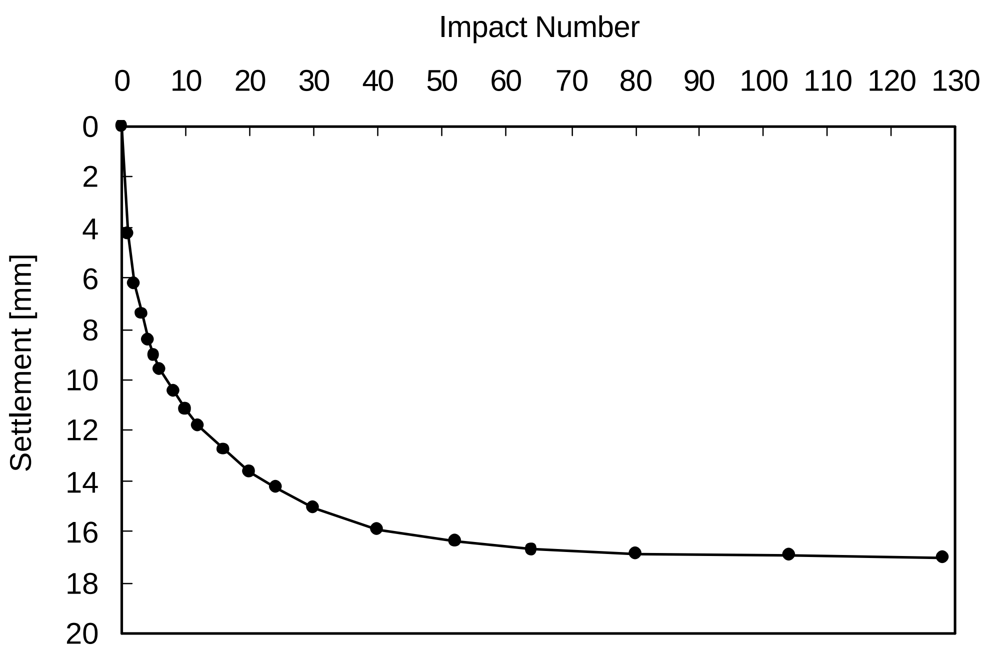

FIG. 8. Settlement versus impact number.

The undrained strength is determined by the initial void ratio. Therefore, the determination of the in-situ void ratio plays a critical role in site assessment and design. This is still a difficult task, even though several relevant techniques are available, including CPT, S-wave velocity, P-wave velocity, electrical resistivity tomography, ground penetrating radar, and time domain reflectometry. At present, none of these techniques can provide the certainty required in the estimation of in-situ void ratio, which is probably ±0.02.

In addition, the spatial distribution of void ratio affects the undrained response, as observed in water gap experiments (e.g. Fiegel and Kutter 1994; Kokusho 1999). The interaction among various temporal and spatial scales involved in dynamic soil response requires further analysis (schematically captured in Figure 9): the seismic wave has its own characteristic period T and an associated wave length l; there is a time scale associated to the acceleration and movement of the mass and there is a time scale for pore pressure dissipation. In addition, the wave length has to be compared to the internal spatial variability in the soil mass and the structure size. From this perspective, the dynamic response still remains a complex phenomenon.

Finally, experimental data gathered in the laboratory show that wave-based methods provide unique insight into the evolution of liquefaction.

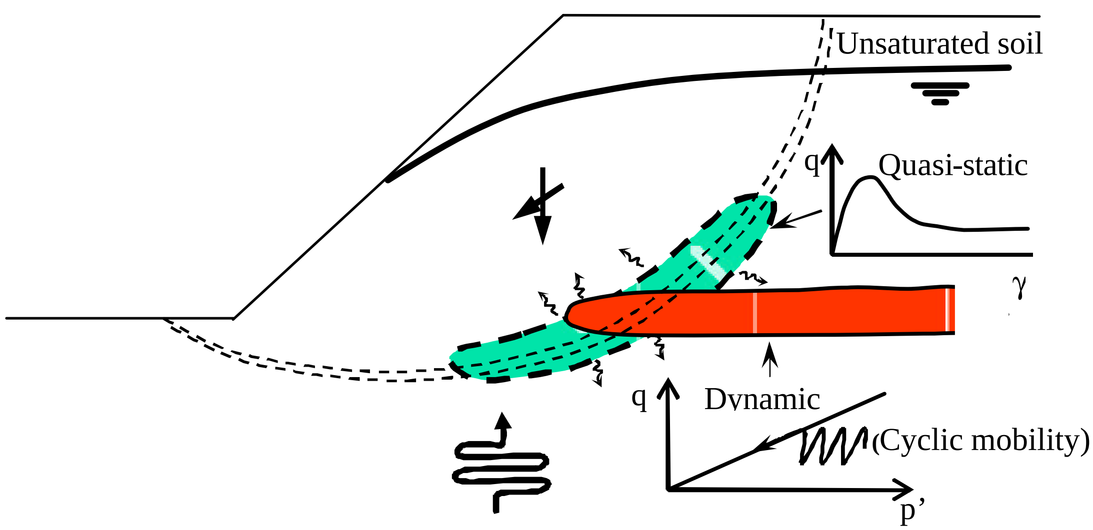

FIG. 9. Macroscale seismic response – Interaction among multiple temporal and spatial scales.

ACKNOWLEDGEMENTS

This study was supported by the NSF-NEES project at UC Davis, NSF project on Scales, Mid-America Earthquake Center, and The Goizueta Foundation.

REFERENCES

Alarcon-Guzman, A., Leonards, G.A., and Chameau, J.L. (1988). "Undrained monotonic and cyclic strength of sand." *J. Geotech. Eng.*, 114(2), 1089-1109.

Been, K. (1999). "The critical state line and its application to soil liquefaction.", *Physics and Mechanics of Soil Liquefaction*, Lade, P.V. and Yamamuro, J.A. eds., Rotterdam, 195-204.

Been, K., Jefferies, M.G., and Hachey, J. (1991). "The critical state of sands.", *Géotechnique*, 41(3), 365-381.

Cho. G.C. (2001). "Unsaturated soil stiffness and post-liquefaction shear strength." PhD thesis, Georgia Institute of Technology, Atlanta, Georgia, 288p.

Dobry, R., Vasquez-Herrera, A., Mohamad, R., and Vucetic, M. (1985). "Liquefaction flow failure of silty sand by torsional cyclic tests." *Advances in the art of testing soils under cyclic conditions*, Proceedings of a session sponsored by the Geotechnical Engineering Division in conjunction with the ASCE Convention in Detroit, Michigan, Khosla eds., 29-50.

Fiegel, G.L., and Kutter, B.L. (1994). "Liquefaction mechanism for layered soils." *J. Geotech. Eng.*, 120(4), 737-755.

Finno, R.J., Viggiani, G., Harris, W.W., and Mooney, M.A. (1998). "Localization of strains in plane strain compression of sand." *Localization and Bifurcation Theory for Soils and Rocks*, Adachi, T., Oka, F., and Yashima, A. eds., 249-257.

Ishihara, K. (1993). "The Rankine Lecture: Liquefaction and flow failure during earthquakes." *Géotechnique*, 43(3), 351-415.

Kokusho, T. (1999). "Water film in liquefied sand and its effect on lateral spread." *J. Geotech. Geoenviron. Eng.*, 125(10), 817-826.

Lee, J.S. (2003). "High resolution geophysical techniques for small-scale soil model testing." PhD Thesis, Georgia Institute of Technology, Atlanta, Georgia, 280p.

Poulos, S.J., Castro, G., and France, J.W. (1985). "Liquefaction evaluation procedure." *J. Geotech. Eng.*, 111(6), 772-792.

Santamarina, J.C., Klein, K.A., and Fam, M.A. (2001). "Soils and waves– particulate materials behavior, characterization and process monitoring." John Wiley and Sons. New York, 488p.

Seed, H.B. (1979). "Soil liquefaction and cyclic mobility evaluation for level ground during earthquakes." *J. Geotech. Eng.*, 105(2), 201-255.

Vaid, Y.P., and Thomas, J. (1995). "Liquefaction and postliquefaction behavior of sand." *J. Geotech. Eng.*, 121(2), 163-173.

Yamamuro, J.A., and Lade, P.V. (1995). "Strain localization in extension tests on granular materials., *J. Engineering Mechanics*, 121(7), 828-836.

Yoshimine, M., Robertson, P.K., and Wride, C.E. (1999). "Undrained shear strength of clean sands to trigger flow liquefaction." *Can. Geotech. J.*, 36, 891-906.

Keywords: Critical State Line. Cyclic Mobility. Flow Liquefaction. P-wave Reflection Imaging. Scales. Shear Wave Velocity. Void Ratio.